Catalysis
Science &
Technology

ROYAL SOCIETY
OF CHEMISTRY

PAPER

View Article Online
View Journal | View Issue

Cite this: *Catal. Sci. Technol.*, 2020, **10**, 2652

Kinetic study of the methane dry (CO_2) reforming reaction over the $Ce_{0.70}La_{0.20}Ni_{0.10}O_{2-\delta}$ catalyst

Lidia Pino, * Cristina Italiano, Massimo Laganà, Antonio Vita and Vincenzo Recupero

Received 30th October 2019,
Accepted 18th March 2020

DOI: 10.1039/c9cy02192b

rsc.li/catalysis

The kinetic behaviour of the $Ce_{0.70}La_{0.20}Ni_{0.10}O_{2-\delta}$ catalyst during the methane dry reforming reaction was investigated in a fixed bed reactor in the temperature range of 923–1023 K with the partial pressure of CH_4 and CO_2 ranging between 5 and 50 kPa. The experimental data were fitted using the empirical power-law rate equation and Langmuir–Hinshelwood kinetic models proposed in literature for the Ni–La_2O_3 catalytic system and based on two-step single- and dual-site mechanisms. The obtained fitting results, after statistical and thermodynamic discrimination, showed that the mechanism of the dry reforming reaction over the $Ce_{0.70}La_{0.20}Ni_{0.10}O_{2-\delta}$ catalyst could be successfully described by the two-step dual-site mechanism. The activation energies for the CH_4 consumption from the power law and Langmuir–Hinshelwood models were estimated to be 91.5 and 136.9 kJ mol^{-1}, respectively. The lower activation energies for the CO_2 consumption (70.2 and 100.6 kJ mol^{-1} from both models) suggested that the CO_2 activation should faster than CH_4. The basic nature of the Ce–La–O sites catalyzed the CO_2 conversion to oxy-carbonate, decreasing the CO_2 activation energy compared to that of CH_4.

1. Introduction

The "Paris Agreement" signed by 195 countries under the United Nations Framework Convention on Climate Change (UNFCC) aims to reduce greenhouse gas emissions, limiting the earth to a 2 °C temperature rise.[1] This ambitious perspective involves, as an energetic strategy, the conversion of the current energetic vector from petroleum to an H_2-based energetic vector, which is widely considered an efficient and clean energy source.[2,3] Indeed, as an energy carrier, hydrogen allows decarbonisation in many sectors like transport, industries, space heating and storage for intermittent renewable energy.[4] In this context, methane dry reforming ($CH_4 + CO_2 \rightarrow 2H_2 + 2CO$, $\Delta H_{298} = 260.5$ kJ mol^{-1}) can be considered as a dual global warming addressing technology as it consumes and/or mitigates two greenhouse gases (CO_2 and CH_4), producing synthesis gas (CO and H_2) with an H_2/CO molar ratio closer to unity. This is adequate for the production of valuable synthetic liquid fuels and oxygenated chemicals *via* oxo- and Fischer–Tropsch synthesis processes.[5,6]

Natural gas with a high CO_2 content yet very abundant in nature[7,8] and biogas produced by the anaerobic digestion of biomass[9,10] can represent significant sources of CO_2 and CH_4. Despite these advantages, methane dry reforming is not yet regarded as an industrially mature process. The main limitation lies in catalyst deactivation occurring as a result of the large amount of carbon deposition due to the high reaction temperature.[11,12]

Generally, two types of supported catalysts have been applied for the dry reforming reaction: noble metal (Pt, Pd, Rh, Ru, Ir, *etc.*)-based and transition metal (Ni, Co, Fe, *etc.*)-based catalysts. Although noble metals have been found to be less sensitive to coke deposition,[13–16] Ni-based catalysts have been largely studied because of its abundance and low cost. However, a propensity for deactivation can be observed that normally takes place due to the sintering, cooking and phase transformation of the active metal during the reaction.[17,18]

Different strategies have been adopted to increase the resistance to coke deposition in Ni-based catalysts:[19] modification by promoters (structural and chemical);[20] selection of suitable supports (CeO_2, MgO, La_2O_3, CeO_2–ZrO_2, TiO_2) able to promote coke gasification by CO_2 activation;[21,22] the investigation of novel Ni-structures such as core–shell, core-tube and mesoporous framework.[23–25] In addition, it has been evidenced that a fine-tuning and intensification of the interactions between Ni and support can induce better anti-coke and anti-sintering performance of the catalysts.[26,27]

The effect of interactions between the active metal and support, as a result of the formation of a solid solution, on the catalysts' performance during dry reforming reaction has been widely evaluated in literature. Excellent activity and stability have been reported by Hu for the NiO–MgO (or CoO–MgO) solid solution;[28] the carbon deposition is inhibited by

---

CNR Istituto di Tecnologie Avanzate per l'Energia "Nicola Giordano", Via S. Lucia 5, 98126 Messina, Italy. E-mail: lidia.pino@itae.cnr.it

the isolation effect of small nickel particles formed on the catalytic surface coupled with the surface basicity of MgO. Sadykov *et al.* showed that a strong interaction of Ni with Ce–Zr–O oxide, as a support in the reduced state, induces a high activity and coking stability of the developed catalyst.[29] Jang *et al.* attributed the excellent activity of the MgO-promoted Ni/$Ce_{0.8}Zr_{0.2}O_2$ sample (equilibrium CH_4 and CO_2 conversion for 200 h without carbon deposition) to the high strength of the interactions between the components.[30] Makri *et al.* pointed out that the metal oxide interface in the Ni/$Ce_{0.8}Pr_{0.2}O_2$ catalyst plays an important role in reducing coke formation under dry reforming conditions.[31]

The catalytic Ni/La–Ce–O_x mixed oxide system has been widely studied by our research group and successfully applied to reforming reactions.[32,33] In particular, the selected $Ce_{0.70}La_{0.20}Ni_{0.10}O_{2-\delta}$ catalyst under appropriate pre-treatment (reduction at 1023 K) exhibited promising activity and stability during the dry reforming reaction.[34] The absence of carbon deposition and stable performance ($CH_{4,\text{conversion}}$ = 73%; $CO_{2,\text{conversion}}$ = 83%) for 50 h on stream at a gas hourly space velocity (GHSV) of 26 400 h^{-1}, were observed. In addition, a negligible amount (0.12–0.20%) was deposited at increasing GHSV (52 800–105 600 h^{-1}) after H_2 pre-reduction of the catalyst at 1023 K. From the characterizations of the catalyst, a complex structure has been highlighted that includes: i) a strong metal support interaction (SMSI) evidenced by the suppression of CO and H_2 chemisorption; ii) the presence of oxygen vacancy defects induced by the partial incorporation of Ni^{2+} in the Ce–La–O_x support with partial exsolution of Ni^{2+} and/or La^{3+} ions from bulk to surface; iii) the bi-functional role of the support, where CeO_2 coupled with La_2O_3 are involved in CO_2 adsorption and coke gasification. All of these features seemed to be responsible for the observed catalytic performance.

Kinetics and mechanistic studies over Ni catalysts have been widely reported in literature, as summarized in some recent reviews.[35,36] In the presence of La_2O_3 as a support, the proposed mechanisms include the presence of a single- or dual-active site, where the dissociation of methane on Ni particles and carbon gasification by adsorbed CO_2 on the support sites are the rate-determining steps.[37,38]

In the current study, kinetic measurements over the $Ce_{0.70}La_{0.20}Ni_{0.10}O_{2-\delta}$ catalyst were performed. The dependency of the reactant consumption rate and product formation rate on the temperature (923–1023 K) and the reactant partial pressure (5–50 kPa) were evaluated. The results were fitted into a power-law model and the cited Langmuir–Hinshelwood models proposed in literature for the two-step single- and dual-site adsorption mechanisms.

To the best of our knowledge, the intrinsic kinetics of the CeO_2–La_2O_3 mixed oxide-supported Ni catalyst for the dry reforming reaction have not been investigated in detail. The purpose of this study is to combine the characterizations and performance test results from previous investigations with the present kinetics data to propose a plausible kinetics model for the reaction.[34]

2. Experimental

2.1 Catalyst preparation

The catalyst, $Ce_{0.70}La_{0.20}Ni_{0.10}O_{2-\delta}$ (3.66 wt% Ni), was prepared by combustion synthesis as previously reported.[33,34] The metal precursors of cerium ammonium nitrate ($(NH_4)_2Ce(NO_3)_6\cdot 6H_2O$), nickel nitrate ($Ni(NO_3)_2\cdot 6H_2O$), and lanthanum nitrate ($La(NO_3)_3\cdot 6H_2O$) with oxalyldihydrazide as fuel ($C_2H_6N_4O_2$, all reagents from Aldrich) were dissolved in a minimum amount of H_2O. The mixture was then transferred into an oven furnace heated at 623 K to allow water evaporation, promoting the combustion reaction. A huge amount of fumes were produced and a few seconds after ignition, a fragile foam was formed that easily crumbled into powder. The obtained sample, heated at 873 K in air to burn off the carbonaceous residues, was tableted, ground and sieved to obtain particles with the required size.

2.2 Kinetic evaluations

Kinetic studies under different conditions were carried out in a continuous-flow quartz reactor (i.d. = 6 mm) placed in an electric oven. The selection of experimental conditions (reported below) was such that the effect of the external/internal mass and heat transfer could be considered negligible. Weighted amounts of the catalyst (0.011–0.044 g) diluted with quartz of the same size (dilution 1 : 5) were loaded in the middle part of the reactor and supported on quartz wool. The reaction temperature was measured/controlled by two k-thermocouples. One of the thermocouples was placed inside a thermowell and centered in the catalyst bed; the other was located at the outlet of the catalytic bed. The catalyst activation before the catalytic tests was carried out *in situ* by treatment with a 25% H_2/N_2 flow (80 ml min^{-1}) at 1023 K for 2 h, and then the temperature was maintained and/or dropped to the desired reaction temperature. The feed was controlled by mass flow controllers, and the products were analyzed with the help of a gas chromatograph (Agilent 6890 Plus) equipped with FID and TCD detectors. Kinetic measurements were performed in the temperature range of 923–1023 K, employing dilute $CH_4 : CO_2 : N_2 = 1 : 1 : 3$ feeds. The partial pressure dependencies were evaluated by maintaining the pressure of one reactant at 20 kPa and varying the pressure of the other reactant between 5 to 50 kPa. N_2, as the balance gas, was adjusted to maintain the overall pressure constant (101.32 kPa). The gas hourly space velocity was controlled at 1.2 × 10^6 h^{-1} using 0.022 g of the catalyst and appropriate feed flows to obtain significantly lower conversion (<15%) than those defined by thermodynamic equilibrium, and the reaction was controlled by kinetics. For each reactant stream and reaction temperature, the kinetic data were collected after the catalyst was stabilized for about 2 h. The reaction rates, based on the reactant consumption and product formation, were calculated by the following equations:

$$r_{\mathrm{CH_4,CO_2}}\left(\mathrm{mol\ g^{-1}\ s^{-1}}\right) = \frac{F_{\mathrm{i,in}} \times \mathrm{Conv._i}}{1000 \times 22.4 \times 60 \times W_{\mathrm{cat.}}} \tag{1}$$

$$r_{\mathrm{H_2,CO}}\left(\mathrm{mol\ g^{-1}\ s^{-1}}\right) = \frac{F_{\mathrm{i,out}}}{1000 \times 22.4 \times 60 \times W_{\mathrm{cat.}}} \tag{2}$$

where $F_{\mathrm{i,in}}$ (mol min^{-1}) is the volume flow rate of the reagent gas, $F_{\mathrm{i,out}}$ (mol min^{-1}) is the volume flow rate of the component i in the outflow gas, Conv.$_{\mathrm{i}}$ is the reagent conversion and $W_{\mathrm{cat.}}$ (g) is the weight of the catalyst.[39]

2.3 Diagnostic tests for mass and heat transfer limitations

In order to evaluate the appropriate experimental conditions under which the effect of the external and internal mass transfer limitations on the methane dry reforming reaction can be considered negligible, preliminary reforming tests were performed by changing the total flow rate and catalyst particle size. The inter-particle limitation tests were performed at a GHSV of 1.2 × 10^6 h^{-1} (reaction conditions: feed composition 20/20/60 vol%; reaction temperature = 923–1023 K, pressure = 101.32 kPa), and showed an invariant rate for flow rates above 200 ml min^{-1}. This indicated that no external limitations existed under those conditions, as shown in Fig. 1a.

At a selected flow rate of 200 ml min^{-1}, the absence of the intra-particle limitations was verified by using different average sizes of the catalyst particles (0.180–0.444 mm). As evidenced in Fig. 1b, the reaction rate results were almost invariant with particle sizes ranging between 0.254 to 0.444 mm. This suggests that the internal mass transfer limitations can be considered negligible. In summary, the mass transfer limitations and diffusion rate-controlling regime were fully excluded for the conditions selected to perform the catalytic tests, *i.e.*, a flow rate of 200 ml min^{-1} and average particle size of 0.254 mm.

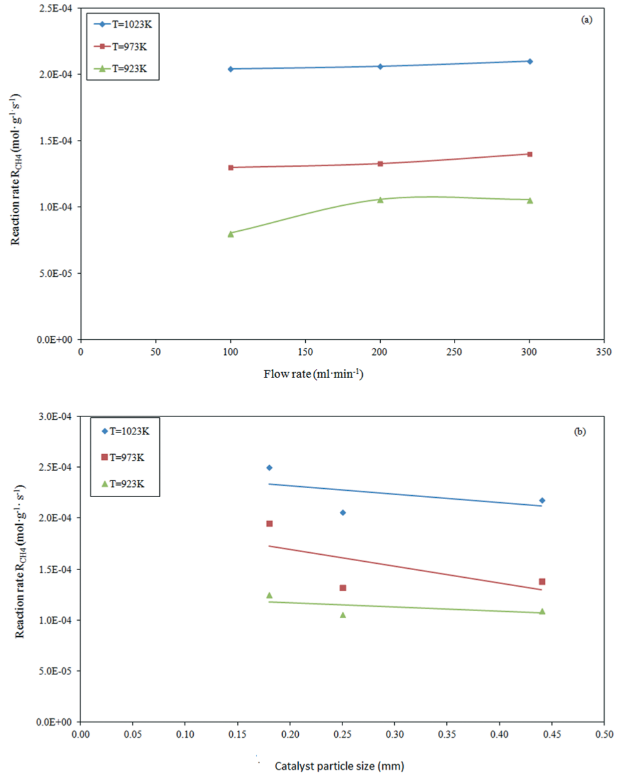

Fig. 1 Effect of volumetric feed flow rate (a) and catalyst particle size (b) on the methane consumption during dry reforming at constant GHSV = 1.2 × 10^6 h^{-1}.

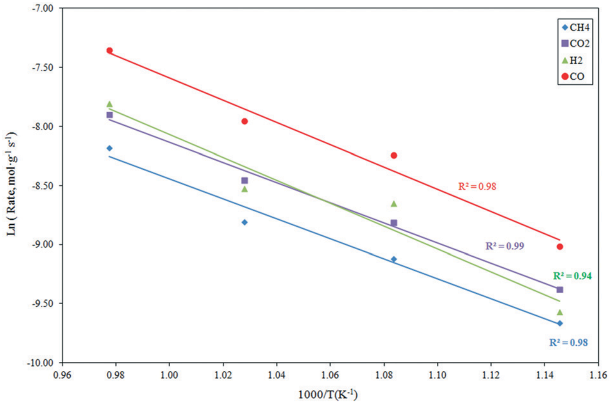

Fig. 2 Influence of the reaction temperature on the CH_4 and CO_2 consumption rate, as well as the H_2 and CO formation rate derived at 101.32 kPa, CH_4 : CO_2 : N_2 = 1 : 1 : 3 and GHSV = 1.2 × 10^6 h^{-1}.

To further investigate the heat and mass transfer limitations for the reaction over the studied catalyst, suitable diagnostic criteria have been also applied. The effect of intra-/interphase heat transfer limitations on the intrinsic kinetics of the reaction was ruled out using the Mears and Anderson criteria, respectively, represented by the following notations:[40,41]

$$\frac{\Delta H \cdot d_{\mathrm{p}} \cdot \mathrm{rate_{exp}} \cdot E_{\mathrm{a}}}{h \cdot R \cdot T^2} < 0.3 \tag{3}$$

$$\frac{\Delta H \cdot {d_{\mathrm{p}}}^2 \cdot \mathrm{rate_{exp}} \cdot E_{\mathrm{a}}}{\lambda_{\mathrm{eff}} \cdot R \cdot T^2} < 0.3 \tag{4}$$

where ΔH is the reaction enthalpy (260 kJ mol^{-1}), rate$_{\mathrm{exp}}$ is the highest reaction rate ($R_{\mathrm{CO_2}}$ = 2.07 × 10^{-4} mol g^{-1} s^{-1}), d_{p} is the catalyst particle diameter (254 × 10^{-6} m), E_{a} is the experimentally derived activation energy (70.17 kJ mol^{-1}), h is the heat transfer coefficient between the gas phase and the catalyst surface (908 W m^2 K), λ_{eff} is the catalyst thermal conductivity (11.71 W m K), R is the universal gas constant and T is the reaction temperature (1023 K). The derived values of 2.4 × 10^{-2} and 4.6 × 10^{-4} suggest that the diagnostic criteria are satisfied; thus, the heat transfer effect was not significant. In addition, the effects of the external mass transfer and intra-phase diffusion were checked by application of the Mears and Weisz–Prater criteria, respectively, that can be defined as follows:[42]

$$\frac{\mathrm{rate_{exp}} \cdot \rho_{\mathrm{s}} \cdot {r_{\mathrm{p}}}^2 \cdot R \cdot T}{p_{\mathrm{CO_2}} \cdot D_{\mathrm{e}}} < 1 \tag{5}$$

$$\frac{\mathrm{rate_{exp}} \cdot \rho_{\mathrm{s}} \cdot d_{\mathrm{p}} \cdot R \cdot T \cdot n}{k_{\mathrm{c}} \cdot p_{\mathrm{CO_2}}} \leq 0.3 \tag{6}$$

Table 1 Comparison of apparent activation energy (E_a, kJ mol^{-1}) over Ni-based catalysts

Catalyst	Temperature (K)	Reagent compositions (kPa) CH$_4$	CO$_2$	N$_2$	E_a (CH$_4$)	E_a (CO$_2$)	E_a (CO)	E_a (H$_2$)	Ref.
$Ce_{0.70}La_{0.20}Ni_{0.10}O_{2-\delta}$	873–1023	20	20	60	70.5	71.0	78.3	80.4	This work
Ni/La_2O_3	773–973				68.0	77.0			38
Ni° from 20 LaNi-SBA(10)	813–893	50	50	—	64.7	57.8	63.7	82.7	47
$Ni/CaO–Al_2O_3$	893–963	50	50		106.7	98.8	103.0	147.4	44
$Ni_{15}CeMgAl$	773–873	20	20	60	65.5	62.2	40.8	61.3	39
$13.5Ni–2K/10CeO_2–Al_2O_3$	873–1073	20	20	60	46.1	46.2	47.4	54.0	45
$1Ce_5Ni_3Mg/Al$	613–673	25	25	50	21.7	23.9			48
Ni–Co/Al–Mg–O	923–1023	62	62	186	69.4	25.9	61.8	85.1	46
$Ni/\gamma Al_2O_3$	773–973	25	25	50	50.9	56.1	80.5		43

where ρ_s is the catalyst particle density (assumed spherical, 2500 kg m^{-3}), n is the reaction order (0.31), p_{CO_2} is the partial pressure of CO_2 at the external surface (20 kPa), k_c is the mass transfer coefficient (0.206 m s^{-1}). Also, in this case, the derived values of 0.18 and 8.4 × 10^{-2}, respectively, confirm a negligible influence of the mass transfer on the reaction rate.

3. Results

3.1 Kinetic evaluations

Apparent activation energy. The effect of the temperature on the reaction rate was investigated in the temperature range 873–1023 K, employing a feed mixture consisting of $CH_4:CO_2:N_2$ = 20:20:60 vol% under a pressure of 101.32 kPa. The results, in the form of an Arrhenius plot, are depicted in Fig. 2. The apparent activation energies estimated for the CH_4 and CO_2 consumption, as well as H_2 and CO formation, are presented in Table 1 and compared with analogous data from Ni-based catalysts derived from literature. As evident, the apparent activation energy can reach very different values over the different catalytic systems applied to the reaction. The support of the Ni catalysts can significantly influence the activation energy by altering the rate-controlling step in the reaction sequence.[45,49] Bradford and Vannice pointed out that the activation energies for the reforming reaction, carried out with Ni catalysts supported on different supports, were typically included in the range 30–100 kJ mol^{-1}. Conversely, high values of up to 160 kJ mol^{-1} have been obtained for some classes of catalysts.[50]

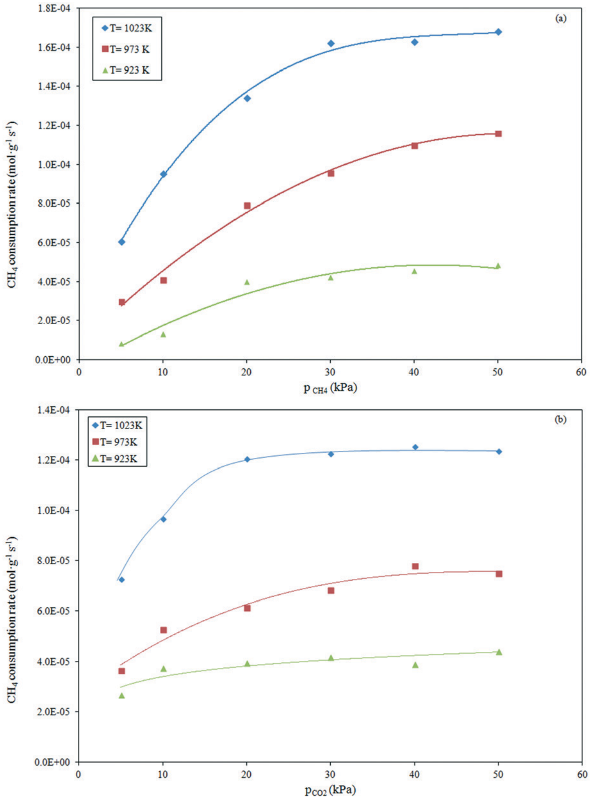

Fig. 3 Effect of variation of partial pressure of CH_4 (a) and CO_2 (b) at constant p_{CO_2} and p_{CH_4}, respectively, on the reaction rate over the $Ce_{0.70}La_{0.30}Ni_{0.10}O_{2-\delta}$ catalyst in the temperature range of 923–1023 K.

In the current investigation with the $Ce_{0.70}La_{0.20}Ni_{0.10}O_{2-\delta}$ catalyst, the activation energies for CH_4 and CO_2 consumption were very close and comparable with analogous data reported by Sierra-Gallego *et al.* for the Ni/La_2O_3 catalytic system.[38] The apparent activation energies for hydrogen and CO were greater than those for CH_4 and CO_2, suggesting that the rate-determining step for CO and H_2 formation are different from those for CH_4 and CO_2 consumption. In addition, the activation energy for H_2 production was higher than that for the formation of CO. This could be related to the parallel occurrence of the reverse water gas shift reaction (RWSR) that influences the reaction mechanism.[45]

Effect of reactant partial pressures on dry reforming rate. The influence of the partial pressure of CH_4 and CO_2 on the reforming rate was evaluated at a pressure of 101.32 kPa in the temperature range of 923–1023 K. The effect of the CH_4 partial pressure on the consumption rate of CH_4 was evaluated at a constant CO_2 partial pressure of 20 kPa as the CH_4 partial pressure was increased from 5 to 50 kPa. The results evaluated at the different temperatures are depicted in Fig. 3a.

As evident, the rate of methane consumption was noticeably influenced by the CH_4 partial pressure over the whole experimental range of 5–30 kPa. A further increase of

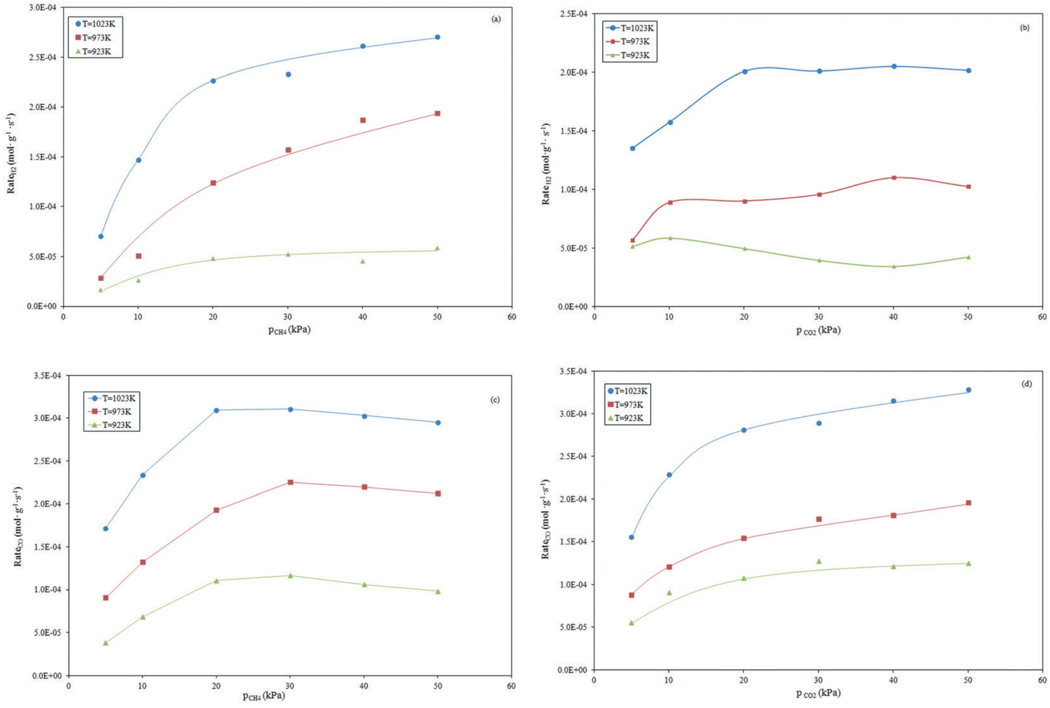

Fig. 4 Effect of the alteration of CH_4 partial pressure (a and c) and CO_2 (b and d) at constant p_{CO_2} and p_{CH_4}, respectively, on the H_2 and CO formation rates.

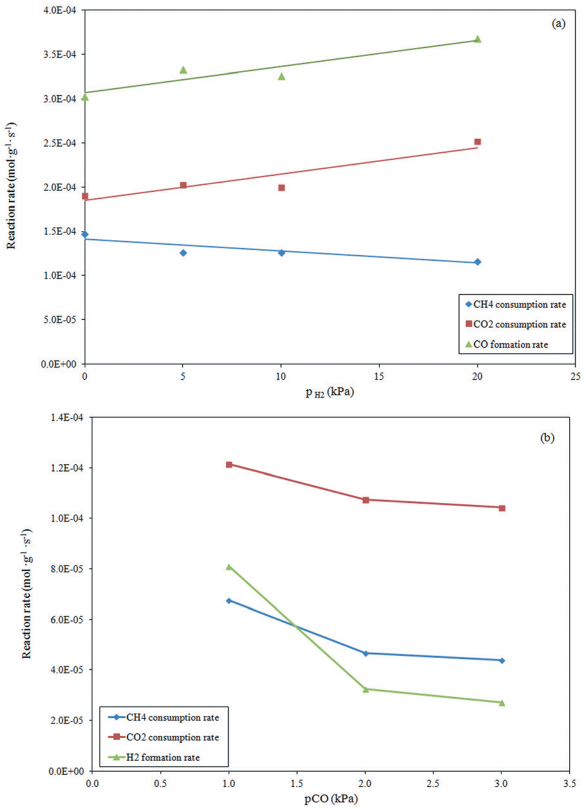

Fig. 5 Influence of H_2 (a) and CO addition (b) to the feed mixture (T = 1023 K, p_{CH_4} = p_{CO_2} = 10 kPa) on the reaction rates.

the CH_4 partial pressure up to 30 kPa induced a less significant effect in the consumption rate. This behavior was observed at high reaction temperatures (973–1023 K). At 923 K, the reforming rate was sensitively affected by the low partial pressures of CH_4 (≤20 kPa), remaining almost unchanged with further increase of the CH_4 partial pressure.

The effect of the variation of the CO_2 partial pressure on the rate of the methane consumption is depicted in Fig. 3b. It can be see that the methane consumption rate increased with increasing CO_2 partial pressure in the range of 5–20 kPa, remaining almost constant at higher partial pressures (20–50 kPa). The relatively constant reaction rate, recorded at all investigated reaction temperatures, can be ascribed to a limitation of the thermodynamic equilibrium of the limiting reactant CH_4 (p_{CH_4} = 20 kPa).

In addition, the effect of the CO_2 partial pressure appeared less significant in the tests carried out at a lower temperature (923 K) in relation to analogous tests at higher temperatures (973–1023 K).

A comparison of Fig. 3a and b suggests that the CH_4 consumption rate was more sensitive to the CO_2 partial pressure than the CH_4 partial pressure at low CH_4 and CO_2 partial pressures, respectively. From these results, a stronger CO_2 adsorption on the catalyst surface can be derived than CH_4 adsorption due to the strong interaction of the CO_2 molecule with the basic surface of the mixed Ni–La–CeO_x oxides, as previous envisaged.[32] The presence of the Ce_2O_3 support from the pre-reduction step of the catalyst can enhance CO_2 adsorption by forming the strong ionic oxide $Ce_2O_2CO_3$. The sequential dissociation of the carbonate

Table 2 Estimation of kinetics parameters from the power law model

Reaction species	Kinetics parameters						
	m	n	A (mol g^{-1} s^{-1}) kPa$^{-(m+n)}$	E_a (kJ mol^{-1})	R^2	Rmsd (mol g^{-1} s^{-1})	σ (mol g^{-1} s^{-1})
CH_4	0.50	0.20	0.66	91.50	0.97	8.6×10^{-6}	4.7×10^{-5}
CO_2	0.29	0.31	0.10	70.17	0.97	9.9×10^{-6}	6.0×10^{-5}
H_2	0.54	0.15	5.62	105.41	0.95	1.7×10^{-5}	1.0×10^{-4}
CO	0.26	0.28	0.53	78.52	0.96	1.8×10^{-5}	7.8×10^{-5}

Rmsd: root mean square deviation; σ: standard deviation.

species into CO_2 and further to CO and O generates oxygen species able to react with carbon deposits at the Ni–$Ce_2O_2CO_3$ interface.[51] Similarly, CO_2 can adsorb onto La_2O_3 (present on the surface) to form La–oxycarbonates, which in turn react with the carbon formed from CH_4 activation at the metal–La interface, cleaning the surface of the catalyst from carbon accumulation. This scavenging effect of the carbonate species on carbon from Ni has been proven to be responsible for the stability evidenced by the Ni/La_2O_3, Rh/La_2O_3 and Rh/La_2O_3–SiO_2 catalysts.[37,44,52–54] Finally, the presence of oxygen vacancies on CeO_2–La_2O_3 in solid solution can promote the dissociation of adsorbed CO_2, generating lattice oxygen that reacts with the carbon atom. This can play a fundamental role in the stability of the doped Ni–CeO_2 catalytic system.[31] Results of the previous investigation with the $Ce_{0.70}La_{0.20}Ni_{0.10}O_{2-\delta}$ catalyst, under analogous experimental conditions after 50 h of reaction, showed the absence of carbon deposition.[34]

Effect of reactant partial pressures on product formation rates. The formation rates of H_2 and CO as a function of the partial pressure of the reactants are depicted in Fig. 4. The rate of H_2 formation for constant CO_2 partial pressure increases linearly by increasing the CH_4 partial pressure in the range 5–20 kPa. A more limited increase at higher CH_4 partial pressure was recorded, as shown in Fig. 4a. This suggests that the dry reforming and RWGS reactions rates become lower in the presence of a limited CO_2 amount. This is supported by the experiments conducted at constant CH_4 partial pressure. Depicted in Fig. 4b, the increase in the CO_2 partial pressure up to the stoichiometric value (20 kPa) involves a noticeable increase in the H_2 formation rates that become invariant at higher partial pressures of CO_2. The equilibrium that is established between H_2 produced by reforming and consumed by RWGS results responsible of the observed trend. The dependence of the CO formation rate on the partial pressures of CH_4 and CO_2, is depicted in Fig. 4c and d, respectively.

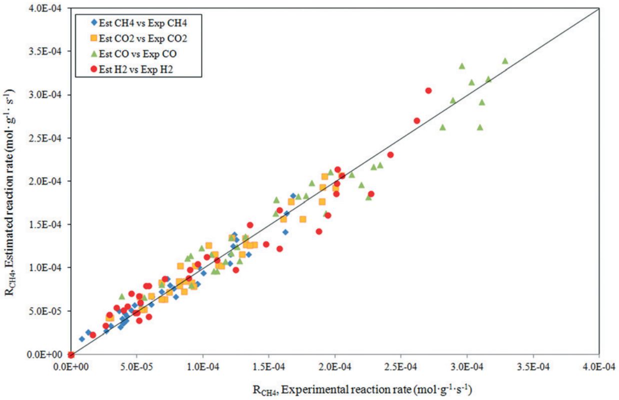

Fig. 6 Statistical fit of the postulated power law model showing the comparison of the rate predicted by the model to the experimental rate.

A quasi-linear dependence of the CO formation rate on the CH_4 partial pressure ranging between 5 to 20 kPa can be observed. Conversely, a light decrease in the CO formation rate at a high partial pressure of CH_4 (Fig. 4c) was observed. This could be due to the effect of side reactions such as RWGS, that limit the CO formation when CO_2 is the limiting reagent. This is supported by the observation of Fig. 4d: the CO formation increases progressively by increasing the partial pressure of CO_2. The observed trend agrees well with those reported by other authors such as Osazuwa *et al.* with the $SmCoO_3$ perovskite catalyst,[55] Nandini *et al.* who evaluated the catalytic activity of a Ni–K/CeO_2–Al_2O_3 sample,[45] and Fan *et al.* who applied a bimetallic Ni–Co/MgO–ZrO_2 catalyst to the dry reforming reaction.[20]

Effect of product partial pressures on dry formation rates. The effect of H_2 in the feed on the dry reforming rate was investigated in the range of 5–20 kPa at a constant CH_4 and CO_2 partial pressure of 10 kPa and reaction temperature of 1023 K. The results depicted in Fig. 5a show that the increase in the H_2 partial pressure induced a light inhibition of the methane consumption rate, while exerting a positive effect on the CO_2 consumption rate and CO production rate. This behavior, attributable to the occurrence of the reverse water gas shift reaction, shows that the Ni–H produced on the surface can reach an equilibrium state with the hydrogen product from the dry reforming reaction.[44]

The effect of the increased CO partial pressure from 1 to 3 kPa in the feed stream on the reaction rates is evidenced in Fig. 5b. The reforming rates were slightly influenced by the CO partial pressure. A decrease in the reforming rate was observed for p_{CO} (up to 2 kPa) that remained almost constant with further increases in the CO partial pressure. Taking in consideration that the CH_4 dissociation and CO adsorption occurred on the Ni active sites, the inhibition effect of CO on the reaction rate was due to the competitive adsorption of CO on active sites that limited the adsorption/dissociation of CH_4 for which the reforming rate decreased. The invariant

Table 3 Activation energy from the power law reported in the literature

Catalyst	Temperature (K)	Partial pressure (kPa)	E_{CH_4} (kJ mol^{-1})	E_{CO_2} (kJ mol^{-1})	E_{CO} (kJ mol^{-1})	E_{H_2} (kJ mol^{-1})	Ref.
10.1Ni/MgO	673–823	5–53	92.10	87.9	87.90	146.51	49
1.22Ni/TiO$_2$	673–823	"	108.8	87.9	96.28	133.95	"
Co/La$_2$O$_3$	923–1023	5–50	96.44	72.22	69.71	101.50	60
Ni/Al$_2$O$_3$	850–1000	17–51	76.0				59
5Ni/CeO$_2$–SiO$_2$-*c*	703–733	20–40	154.7				61
5Ni/CeO$_2$–SiO$_2$-*p*	"	"	97.3				"
4.7Ni/ZnO	863–883	4.5–11	110.7	118.4			62
4.8Ni–4.3MgO/ZnO	743–763	"	97.4	106.3			"

Table 4 Langmuir–Hinshelwood kinetic models parameters

Model no.	Temperature (K)	Kinetic constant						
		K_1 (kPa^{-1})	k_2 (mol g^{-1} s^{-1})	K_3 (kPa^{-1})	k_4 (mol g^{-1} s^{-1})	R^2	Rmsd (mol g^{-1} s^{-1})	σ (mol g^{-1} s^{-1})
1	1023	0.0323 (1.8 × 10^{-2})	0.00036 (1.5 × 10^{-4})	0.0037 (3.5 × 10^{-1})	0.00815 (7.0 × 10^{-2})	0.97	2.3 × 10^{-5}	2.6 × 10^{-3}
	973	0.0250 (1.3 × 10^{-2})	0.00025 (9.4 × 10^{-5})	0.0080 (1.0 × 10^{-1})	0.00267 (3.4 × 10^{-1})	0.96	3.0 × 10^{-6}	7.5 × 10^{-6}
	923	0.0811 (5.4 × 10^{-2})	0.00005 (1.8 × 10^{-5})	0.0100 (3.0 × 10^{-2})	0.00299 (8.1 × 10^{-3})	0.91	7.9 × 10^{-6}	1.8 × 10^{-5}
2	1023	0.0285 (2.7 × 10^{-2})	0.00040 (3.2 × 10^{-5})	0.0069 (2.5 × 10^{-2})	0.0043 (1.4 × 10^{-3})	0.97	1.5 × 10^{-5}	8.7 × 10^{-4}
	973	0.0466 (5.4 × 10^{-2})	0.00019 (1.8 × 10^{-4})	0.0100 (9.0 × 10^{-2})	0.0024 (1.1 × 10^{-3})	0.93	1.4 × 10^{-5}	2.8 × 10^{-4}
	923	0.0679 (7.7 × 10^{-2})	0.00007 (5.6 × 10^{-5})	0.0181 (3.2 × 10^{-1})	0.0012 (8.2 × 10^{-4})	0.92	2.4 × 10^{-6}	4.8 × 10^{-6}

Rmsd: root mean square deviation. σ: standard deviation, (values in parenthesis are the standard deviation for the kinetic constants).

Table 5 Models screening using change in entropies and enthalpies for CH_4 and CO_2

Reagent	Model no.	ΔH (kJ mol^{-1})	ΔS (kJ mol^{-1} K)	R^2	Criteria (eqn (20))
CH_4	1	−74.04	−102.92	0.58	$10 \leq 102.92 \leq 115.85$ (yes)
	2	−68.84	−97.87	0.98	$10 \leq 97.87 \leq 108.58$ (yes)
CO_2	1	−77.25	−121.20	0.89	$10 \leq 121.20 \leq 120.35$ (no)
	2	−76.49	−117.21	0.99	$10 \leq 117.21 \leq 119.30$ (yes)

CH_4 consumption rate observed at high CO partial pressure can suggest a limited CO adsorption on the Ni active sites.

3.2 Kinetic modeling

Power law model. The obtained kinetic data, including the reaction rates and partial pressures of the reactants (CH_4 and CO_2), were first fitted into the empirical power law model. This provides a rough estimation of the reaction parameters even though it does not account for the reaction mechanisms. The empirical power law model for the dry reforming reaction is given in the following equation:

$$r_{\mathrm{i}} = A\exp\left(\frac{-E_{\mathrm{a}}}{RT}\right)p_{\mathrm{CH_4}}^{m}pP_{\mathrm{CO_2}}^{n} \tag{7}$$

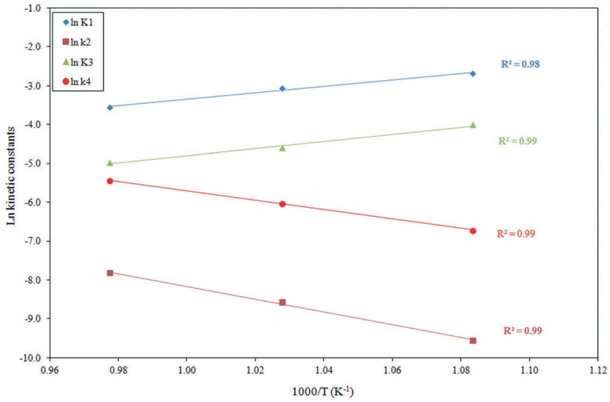

Fig. 7 Effect of the temperature on the adsorption (K_1 and K_3) and reaction constants (k_2 and k_4) for the Langmuir–Hinshelwood kinetic model (model 2).

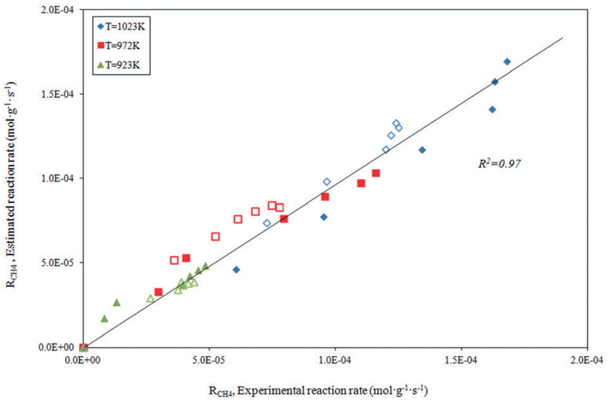

Fig. 8 Statistical fit of the postulated model 2 comparing the rate predicted by the model to the experimental rate.

where r_i represents the consumption rates of CH_4 and CO_2, as well as the formation rates of H_2 and CO; A represents the pre-exponential factor, E_a is the activation energy; R is the universal gas constant; p_{CH_4} and p_{CO_2} are the partial pressures of CH_4 and CO_2, respectively, with m and n as the related reaction orders; and T is the absolute reaction temperature.

The SOLVER function, available in Excel spreadsheets, was employed to evaluate the kinetic parameters from the nonlinear power law model.[56,57] The goodness of fit was determined by the coefficient of determination (R^2). The estimated values of the kinetic parameters, as well as the corresponding R^2, Rmsd (residual sum of square) and σ (standard deviation) values are summarized in Table 2. It can be seen that the reaction rates for the reactants and products were satisfactorily predicted with $R^2 \geq 0.95$.

Activation energies of approximately 91.5 kJ mol^{-1} and 70.17 kJ mol^{-1} were derived for CH_4 and CO_2 consumption, respectively, as evidenced in Table 2. The activation energy of the CH_4 consumption was higher than that of the CO_2 consumption. This indicates that the CH_4 activation is more temperature-sensitive than that of CO_2.

The lower CO_2 activation energy related to the methane activation energy implied furthermore that the rate of CO_2 consumption was faster than that for CH_4. Thus, the CO_2 conversion was higher than the CH_4 conversion.[58]

The reaction orders obtained for the CH_4 consumption (m = 0.50; n = 0.20) indicate that the CH_4 partial pressure significantly influences the methane reforming. In addition, the CO_2 consumption is influenced by the CO_2 partial pressure (m = 0.29; n = 0.31).

The activation energies of H_2 (105.41 kJ mol^{-1}) and CO (78.52 kJ mol^{-1}) are comparable to that of CH_4 and CO_2, respectively. Therefore, it can be derived that the H_2 formation was predominantly influenced by CH_4, while the CO formation was primarily influenced by CO_2. Furthermore, both values were higher than those for the CH_4 and CO_2 consumption. This suggests, as previously observed, that the rate-determining steps for the H_2 and CO formation are different from those for the reagent consumption.

The activation energy for H_2 production, noticeably higher than that CO, is a clear indication of the influence of the RWGS reaction on the H_2 formation. A comparison of the experimental rates for CH_4 and CO_2 consumption, as well as for the H_2 and CO formation with those predicted by the power law model, are given in Fig. 6. A good agreement between the predicted and experimental values emerged.

The derived kinetic parameters are very similar to the reported values by Bradford and Vannice[49] and Ayodele *et al.* for the reaction carried out with Ni/MgO and Co/La_2O_3,[60] respectively, as evidenced in Table 3. Its results are noticeably higher than the activation energy reported by Takano *et al.* over a traditional Ni/Al_2O_3 (cordierite) catalyst.[59] Although the different supports have different influences on the activity of the metallic phase, this could be ascribed to the high interaction occurring between Ni and the La–CeO_x support.

Indeed, Bradford and Vannice pointed out that with the Ni–TiO_2 catalyst, the SMSI induced a noticeable value of the activation energy (108 kJ mol^{-1}) that increased to 171.6 kJ mol^{-1} after 18 h of stream.[49] In this case, the migration of TiO_x on the Ni surface may increase the activation barrier for methane dissociation. Recently, Yan *et al.* showed that the close metal–support interface between Ni and CeO_2 in the Ni–CeO_2–SiO_2 catalyst led to a substantial decrease in the activation energy from 154.7 kJ mol^{-1} (Ni–CeO_2–SiO_2 sample *C*) to 97.3 kJ mol^{-1} with the sample in the absence of interactions (Ni–CeO_2–SiO_2 sample *P*).[61] Analogous evidence emerged from the study reported by Singha *et al.*, where the methane activation energy of the Ni/ZnO catalyst decreased significantly from 110.7 kJ mol^{-1} to 97.4 kJ mol^{-1} by the addition of MgO in the catalyst formulation, inducing high Ni dispersion and metal–support interactions.[62] Therefore, other models may be more appropriate than the power law. In the following section, the Langmuir–Hinshelwood mechanism models proposed in the literature for the Ni–La_2O_3 catalytic system (and as previously mentioned) were applied to evaluate the kinetic mechanism of the current sample.

Langmuir–Hinshelwood models. Many studies related to the kinetics of methane reforming with CO_2 are generally based on mechanistic steps that include: i) the dissociation/activation of CH_4 and CO_2; ii) adsorption of elemental and intermediate species on active sites; iii) formation of products *via* surface reactions; iv) desorption of product species.[63] The fundamental study carried out by L. M. Aparicio showed that there is not a single rate-determining step (RDS) in the reaction.[64] Therefore, in most cases, the CH_4 and CO_2 dissociation or activation are considered to be the RDS.

Based on DRIFT (diffuse reflectance infrared Fourier transform) and SSITKA (steady-state isotopic transient kinetic analysis) studies, Verykios and co-workers proposed a mechanistic sequence for the Ni/La_2O_3 catalytic system where CH_4 cracking is a slow step, while the CH_4 adsorption is at equilibrium.[65–67] The strong interaction occurring between CO_2 and La_2O_3 that leads to the formation of the $La_2O_2CO_3$ species, can be considered a fast step at equilibrium. Conversely, the reaction between this formed species with Ni particles at the Ni/$La_2O_2CO_3$ interface oxygenated species becomes a slow step.[37]

This mechanistic step can be synthetically represented by the following reactions:

$$CH_4 + S \overset{K1}{\leftrightarrow} CH_4\text{–}S(\text{equilibrium}) \tag{8}$$

$$CH_4\text{–}S \overset{k2}{\rightarrow} C\text{–}S + 2H_2(\text{RDS}) \tag{9}$$

$$CO_2 + La_2O_3 \overset{K3}{\leftrightarrow} La_2O_2CO_3(\text{equilibrium}) \tag{10}$$

$$La_2O_2CO_3 + C\text{–}S \overset{k4}{\rightarrow} La_2O_3 + 2\,CO + S(\text{RDS}) \tag{11}$$

$$H_2 + 2\text{–}S \leftrightarrow 2H\text{–}S(\text{equilibrium}) \tag{12}$$

In addition, the simultaneous occurrence of RGSR includes the sequence of the following reaction steps:

$$CO_2 + S \leftrightarrow S\text{–}CO_2(\text{equilibrium}) \tag{13}$$

$$S\text{–}CO_2 + H\text{–}S \rightarrow S\text{–}CO + OH\text{–}S(\text{slow}) \tag{14}$$

$$S\text{–}OH + H\text{–}S \leftrightarrow 2S\text{–}H_2O(\text{equilibrium}). \tag{15}$$

On this basis, the authors derived the following rate expression for the methane consumption:

$$r_{CH_4} = \frac{K_1 k_2 K_3 k_4 p_{CH_4} p_{CO_2}}{K_1 K_3 k_4 p_{CH_4} p_{CO_2} + K_1 k_2 p_{CH_4} + K_3 k_4 p_{CO_2}} \qquad \textbf{(Model 1)}$$

where K_1 is the adsorption equilibrium constant for CH_4; k_2 is the rate constant of methane cracking on the metallic surface; K_3 is the adsorption equilibrium constant of the reaction between CO_2 and La_2O_3; k_4 is the rate constant of the reaction between the oxycarbonate species and carbon deposited on the Ni surface.

Sierra-Gallego *et al.* studied the kinetic behaviour of the Ni/La_2O_3 catalyst obtained from the reduction of $LaNiO_3$ perovskite structure.[38] From XPS (X-ray photoelectron spectroscopy) after the catalytic tests, the authors derived that the Ni particles were partially covered by the $La_2O_2CO_3$ species due to the migration of La_2O_3 over the metal particles. From this evidence, the authors developed a rate reaction equation including, for the first time, the presence of two active sites on the catalyst surface: metallic nickel particles and the La_2O_3 metal support. Assuming a negligible H_2 and CO surface coverage, the proposed dual active-site mechanism involves the following steps:

$$CH_4 + S_1 \overset{K1}{\leftrightarrow} CH_4\text{–}S_1(\text{equilibrium}) \tag{16}$$

$$S_1\text{–}CH_4 \overset{k2}{\rightarrow} S_1\text{–}C + 2H_2(\text{RDS}) \tag{17}$$

$$CO_2 + S_2 \overset{K3}{\leftrightarrow} S_2\text{–}CO_2(\text{equilibrium}) \tag{18}$$

$$S_2\text{–}CO_2 + S_1\text{–}C \overset{k4}{\rightarrow} S_2 + 2CO + S_1(\text{RDS}) \tag{19}$$

where S_1 represents the metallic active site (Ni°) and S_2 is the La_2O_3 support as the active site. The related rate model assumes the following form:

$$r_{CH_4} = \frac{K_1 k_2 K_3 k_4 p_{CH_4} p_{CO_2}}{K_3 k_4 p_{CO_2} + K_1 K_3 k_4 p_{CH_4} p_{CO_2} + K_1 k_2 p_{CH_4} + K_1 k_2 K_3 p_{CO_2}} \qquad \textbf{(Model 2)}$$

The current catalytic system can be envisaged as a Ni-solid solution with ceria–lanthana in which the presence of anionic vacancies can help the abstraction of H species from CH_4. The sequential decomposition of the CH_3 intermediate into C, that could substitute steps 9/17 in previous models and is described as:

$$S\text{–}CH_4 \rightarrow S\text{–}CH_x + \frac{(4-x)}{2} H_2, \tag{9a, 17a}$$

occurs very fast. The reversible CO_2 adsorption on the support surface can happen on both La_2O_3 and Ce_2O_3, generating carbonate species at the boundary of Ni particles. The subsequent reaction with adsorbed carbon generates CO, restoring the active sites.

The presence of oxygen vacancies (□) on the ceria–lanthana support contributes to the CO_2 adsorption/dissociation step:

$$CO_2 + \square \rightarrow CO + O_{\text{lattice}}$$

Diffusion of the generated lattice oxygen towards the Ni surface exerts a promoting effect in the cleaning steps (carbon oxidation to CO) of the surface sites envisaged in the reaction sequences.

On this basis, the kinetic models proposed by Verykios's group (model 1) and Sierra-Gallego *et al.* (model 2) were applied to fit the experimental data obtained from this study over the $Ce_{0.70}La_{0.20}Ni_{0.10}O_{2-\delta}$ catalyst. The parameters of both models were estimated using the nonlinear regression method with the ANEMONA.XLS tools, an Excel template previously developed and successfully tested with some kinetic models applied in literature for the dry reforming reaction.[68]

The summary of the kinetic parameters estimated from the two Langmuir–Hinshelwood rate expressions are summarized in Table 4. As evident, both models gave fitting regression coefficients (R^2) greater than 0.90, which can be considered to be a good fitting. Thus, the models are statistically significant.

In order to evaluate the related thermodynamic relevance, the models were further screened by application of the criteria designed to evaluate the adsorption equilibrium constants obtained in a Langmuirian rate expression, defined by the following equation:[69]

$$10 \le -\Delta S \le 12.2 - 0.0014\Delta H \tag{20}$$

where ΔS and ΔH are the changes in entropy and enthalpy, respectively. However, the change in the entropies and enthalpies have been estimated using the Van't Hoff expression:

$$\ln K_i = \frac{-\Delta H_i}{RT} + \frac{\Delta S_i}{R} \tag{21}$$

where K_i is the adsorption constant (K_1 for CH_4 or K_3 for CO_2). The derived thermodynamic parameters for CH_4 and CO_2 and the related evaluations are synthesized in Table 5. As evident, model 2 emerges as the best kinetic model that represents the mechanism of the reaction: it satisfies the thermodynamic criterion, the R^2 values (0.98 and 0.99) are considerably higher than the corresponding values derived for model 1 (0.58 and 0.89) that failed to satisfy the thermodynamic criteria.

The temperature dependence of the reaction rate parameters derived from model 2 is shown in the following equations obtained from the Arrhenius plots (depicted in Fig. 7) of the K_1, k_2, K_3 and k_4 constants:

$$K_1 = 7.82 \times 10^{-6} \exp(8280/T) \tag{22}$$

$$k_2 = 4.80 \times 10^{3} \exp(-16\,470/T) \tag{23}$$

$$K_3 = 7.54 \times 10^{-7} \exp(9200/T) \tag{24}$$

$$k_4 = 6.32 \times 10^{2} \exp(-12\,110/T). \tag{25}$$

The adsorption equilibrium constants K_1 and K_3 increase with decreasing reaction temperature, as expected since the CH_4 and CO_2 adsorptions are exothermal processes. The reaction rate constants k_2 and k_4 follow an opposite trend. It is interesting to note that the k_4 values are noticeably higher than the k_2 rate constants related to the methane cracking. From this, it is possible to derive that the catalysts kinetically inhibited the carbon deposition in accordance with analogous observations reported by other authors.[20,39]

The absence of the carbon deposition observed in all experimental tests suggests that the catalyst stabilizes CH_x decomposition and CO disproportion that is likely the mechanism for carbon deposition during the dry reforming reaction.[49] The ability to activate the C–H bond cleavage requires the electron pair donation from CH_4 to the unfilled d-orbital of nickel. The high d-electron density of the Ni atoms, as previously revealed by XPS studies, inhibits this process.[34] Similarly, the evidenced suppression of CO chemisorptions shown by this catalytic system may increase the activation barrier for CO dissociation.

The activation energies related to CH_4 and CO_2 were 136.9 and 100.6 kJ mol^{-1}, respectively, which are higher than the corresponding values derived with the power law rate expression. This is reasonable considering that the Langmuir–Hinshelwood rate expression takes into account the adsorption/desorption enthalpies. Thus, the predicted values are expected to be higher than the power law expression.[70]

The parity plot showing the comparison between the experimental and predicted CH_4 reaction rates is shown in Fig. 8. The kinetic model shows a good fit with the experimental data with a correlation coefficient of $R^2 = 0.97$.

Conclusions

The kinetics of methane dry reforming over the $Ce_{0.70}La_{0.20}Ni_{0.10}O_{2-\delta}$ catalyst has been evaluated at CH_4 and CO_2 partial pressures ranging between 5 to 50 kPa at 923, 973 and 1023 K. The reaction mechanism was proposed on the basis of literature and experimental observations.

The experimental data were fitted into the power law and Langmuir–Hinshelwood kinetics expression considering a dual-step with single-(Ni°) and dual-active sites (La_2O_3 support), respectively, for the reaction. The discrimination between the two models, statistically and thermodynamically, was evidenced as the reaction mechanism of the dry reforming reaction over the $Ce_{0.70}La_{0.20}Ni_{0.10}O_{2-\delta}$ catalyst. It can be described by a dual molecular adsorption of both CH_4 and CO_2 on metallic nickel and support (La_2O_3), respectively, with surface reactions as the rate-determining steps. The reaction between CO_2 and support generates the $La_2O_2CO_3$ species, and is able to react with carbon at the metal–carbon interface to produce CO and clean up the metallic surface.

The high value of the kinetic constant k_4 (reaction between carbonate species and carbon deposited) compared with k_2 (methane cracking) suggests that the catalyst kinetically inhibits the excess of carbon deposition.

Conflicts of interest

There are no conflicts to declare.

References

1 United Nations Framework Convention on Climate Change (UNFCC), Adoption of the Paris Agreement, Report N. FCCC/CP/2015, http://Unounfccc.int/resource/docs/2015/cop21/eng/l09r01.pdf.

2 J. D. Fonseca, M. Camargo, J.-M. Commenge, L. Falk and I. D. Gil, *Int. J. Hydrogen Energy*, 2019, **44**, 9486–9504.

3 G. Sdanghi, G. Maranzana, A. Celzard and V. Fierro, *Renewable Sustainable Energy Rev.*, 2019, **102**, 150–170.

4 A. Chapman, K. Itaoka, K. Hirose, F. T. Davidson, K. Nagasawa, A. C. Lloyd, M. E. Webber, Z. Kurban, S. Managi, T. Tamaki, M. C. Lewis, R. E. Hebner and Y. Fujii, *Int. J. Hydrogen Energy*, 2019, **44**, 6371–6382.

5 K. Nagaoka, K. Takanabe and A. Ken-Ichi, *Appl. Catal., A*, 2003, **255**, 13–21.

6 S. A. Chattanathan, S. Adhikari and S. Taylor, *Int. J. Hydrogen Energy*, 2012, **37**, 18031–18039.

7 R. Nehring, *Philos. Trans. R. Soc., B*, 2009, **364**, 3067–3079.

8 J.-M. Lavoie, *Front. Chem.*, 2014, **2**, B1.

9 Y. Gao, J. Jianga, Y. Meng, F. Yan and A. Aihemaiti, *Energy Convers. Manage.*, 2018, **171**, 133–155.

10 V. Nallathamb Gunaseelan, *Biomass Bioenergy*, 1997, **13**, 83–114.

11 S. Gaur, D. J. Haynes and J. J. Spivey, *Appl. Catal., A*, 2011, **403**, 142–151.

12 A. Fouskas, M. Kollia, A. Kambolis, C. Papadopoulou and H. Matralis, *Appl. Catal., A*, 2013, **474**, 125–134.

13 J. H. Bitter, K. Sehan and J. A. Lercher, *J. Catal.*, 1991, **183**, 336–343.

14 F. Menegazzo, M. Signoretto, F. Pinna, P. Canton and N. Pernicone, *Appl. Catal., A*, 2012, **439–440**, 80–87.

15 D. Pakhare and J. Spivey, *Chem. Soc. Rev.*, 2014, **43**, 7813–7837.

16 F. Wang, L. Xu, W. Shi, J. Zhang, K. Wu, Y. Zhao, H. Li, H. X. Li, G. Q. Xu and W. Chen, *Nano Res.*, 2017, **10**, 364–380.

17 M. Usman, W. M. A. Wan Daud and H. F. Abbas, *Renewable Sustainable Energy Rev.*, 2015, **45**, 710–744.

18 G. Zhang, J. Liu, Y. Xu and Y. Sun, *Int. J. Hydrogen Energy*, 2018, **43**, 15030–15054.

19 S. Arora and R. Prasad, *RSC Adv.*, 2016, **6**, 108668–108688.

20 M.-S. Fan, A. Z. Abdullah and S. Bhatia, *ChemCatChem*, 2009, **1**, 192–208.

21 W.-J. Jang, J.-O. Shim, H.-M. Kim, S.-Y. Yoo and H.-S. Roh, *Catal. Today*, 2019, **324**, 15–26.

22 I. Luisetto, S. Tuti, C. Romano, M. Boaro, E. Di Bartolomeo, J. Kopula Kesavan, S. M. Senthil Kumar and K. Selvakumar, *J. CO2 Util.*, 2019, **30**, 63–78.

23 S. Das, J. Ashok, Z. Bian, N. Dewangan, M. H. Wai, Y. Du, A. Borgna, K. Hidajat and S. Kawi, *Appl. Catal., B*, 2018, **230**, 220–236.

24 Y. Lu, D. Guo, Y. Ruan, Y. Zhao, S. Wang and X. Ma, *J. CO2 Util.*, 2018, **24**, 191–199.

25 Z. Li, M. Li, Z. Bian, Y. Kathiraser and S. Kawi, *Appl. Catal., B*, 2016, **188**, 324–341.

26 M. Steib, Y. Lou, A. Jentys and J. A. Lercher, *ChemCatChem*, 2017, **9**, 3809–3813.

27 M. Shah, S. Das, A. K. Nayak, P. Mondal and A. Bordoloi, *Appl. Catal., A*, 2018, **556**, 137–154.

28 Y. H. Hu, *Catal. Today*, 2009, **148**, 206–211.

29 V. A. Sadykov, M. N. Simonov, N. V. Mezentseva and S. N. Pavlova, *et al.*, *Open Chem.*, 2016, **14**, 363–376.

30 W.-J. Jang, D.-W. Jeong, J.-O. Shim, H.-M. Kim, W.-B. Han, J. W. Bae and H.-S. Roh, *Renewable Energy*, 2015, **79**, 91–95.

31 M. M. Makri, M. A. Vasiliades, K. C. Petallidou and A. M. Efstathiou, *Catal. Today*, 2015, **259**, 150–164.

32 L. Pino, A. Vita, F. Cipiti, M. Laganà and V. Recupero, *Appl. Catal., B*, 2011, **104**, 64–73.

33 L. Pino, A. Vita, M. Laganà and V. Recupero, *Appl. Catal., B*, 2014, **148–149**, 91–105.

34 L. Pino, C. Italiano, A. Vita, M. Laganà and V. Recupero, *Appl. Catal., B*, 2017, **218**, 779–792.

35 Y. Kathiraser, U. Oemar, E. T. Saw, Z. Li and S. Kawi, *Chem. Eng. J.*, 2015, **278**, 62–78.

36 G. Zhang, J. Liu, Y. Xu and Y. Sun, *Int. J. Hydrogen Energy*, 2018, **42**, 15030–15054.

37 V. A. Tsipouriari and X. E. Verykios, *Catal. Today*, 2001, **64**, 83–90.

38 G. Sierra Gallego, C. Batiot-Dupeyrat, J. Barrault and F. Mondrago, *Ind. Eng. Chem. Res.*, 2008, **47**, 9272–9278.

39 Z. Bao, Y. Lu and F. Yu, *AIChE J.*, 2017, **63**, 2019–2029.

40 D. E. Mears, *Ind. Eng. Chem. Process Des. Dev.*, 1971, **10**, 541–547.

41 M. E. Davis and R. J. Davis, *Fundamental of chemical reaction engineering*, McGraw-Hill, New York, 2003, pp. 184–239.

42 P. B. Weisz and C. D. Prater, *Adv. Catal.*, 1954, **6**, 143–196.

43 S. Wang and G. Q. Lu, *Ind. Eng. Chem. Res.*, 1999, **38**, 2615–2625.

44 A. A. Lemonidou and I. A. Vasalos, *Appl. Catal., A*, 2002, **228**, 227–235.

45 A. Nandini, K. K. Pant and S. C. Dhingra, *Appl. Catal., A*, 2006, **308**, 119–127.

46 J. Zhang, H. Wang and A. K. Dalai, *Ind. Eng. Chem. Res.*, 2009, **48**, 677–684.

47 J. Dacquin, D. Sellam, C. Batiot-Dupeyrat, A. Tougerti, D. Duprez and S. Royer, *ChemSusChem*, 2014, **7**, 631–637.

48 S. Das, S. Thakur, A. Bag, M. S. Gupta, P. Mondal and A. Bordoloi, *J. Catal.*, 2015, **330**, 46–60.

49 M. C. J. Bradford and M. A. Vannice, *Appl. Catal., A*, 1996, **142**, 97–122.

50 M. C. J. Bradford and M. A. Vannice, *Catal. Rev.: Sci. Eng.*, 1991, **41**, 1–42.

51 F. A. J. Al-Doghachi, U. Rashid, Z. Zainal, M. I. Saiman and Y. H. T. Yap, *RSC Adv.*, 2015, **5**, 81739–81752.

52 X. E. Verikyos, *Int. J. Hydrogen Energy*, 2003, **28**, 1045–1063.

53 J. F. Munera, S. Irusta, L. M. Cornaglia, E. A. Lombardo, D. V. Cesar and M. Schmal, *J. Catal.*, 2007, **245**, 25–34.

54 J. F. Munera, L. Cornaglia, D. V. Cesar, M. Schmal and E. A. Lombardo, *Ind. Eng. Chem. Res.*, 2007, **46**, 7543–7549.

55 O. U. Osazuwa, H. D. Setiabudi, S. Abdullah and C. K. Cheng, *Int. J. Hydrogen Energy*, 2017, **42**, 9707–9721.

56 A. M. Brown, *Comput. Methods Programs Biomed.*, 2001, **65**, 191–200.

57 M. D. A. Hossain, H. H. Ngo and W. Guo, *J. Water Sustainability*, 2013, **3**, 223–237.

58 V. C. H. Kroll, G. J. Tjatjopoulos and C. Mirodatos, *Natural Gas Conversion V. (Stud. Surf. Sci. Catal.)*, 1998, vol. 119, pp. 753–758.

59 A. Takano, T. Tagawa and S. Goto, *J. Chem. Eng. Jpn.*, 1994, **27**, 727–731.

60 B. Ayodele, M. R. Khan, S. S. Lam and C. K. Cheng, *Int. J. Hydrogen Energy*, 2016, **41**, 4603–4615.

61 X. Yan, T. Hu, P. Liu, S. Li, B. Zhao, Q. Zhang, W. Jiao, S. Chen, P. Wang, J. Lu, L. Fan, X. Deng and Y.-X. Pan, *Appl. Catal., B*, 2019, **246**, 221–231.

62 R. K. Singha, A. Yadav, A. Agrawal, A. Shukla, S. Adak, T. Sasaki and R. Bal, *Appl. Catal., B*, 2016, **191**, 165–178.

63 U. Oemar, Y. Kathiraser, L. Mo, X. K. Ho and S. Kawi, *Catal. Sci. Technol.*, 2016, **6**, 1173–1186.

64 L. M. Aparicio, *J. Catal.*, 1997, **165**, 262–274.

65 Z. Zhang, X. E. Verykios, S. M. MacDonald and S. Affrossman, *J. Phys. Chem.*, 1996, **100**, 744–754.

66 V. A. Tsipouriari and X. E. Verykios, *J. Catal.*, 1999, **187**, 85–94.

67 A. Slagtern, Y. Schuurman, C. Leclercq, X. Verykios and C. Mirodatos, *J. Catal.*, 1997, **172**, 118–126.

68 L. Pino, V. Recupero and A. Hernández, *ChemEngineering*, 2018, **2**, 57.

69 M. A. Vannice, *Kinetics of catalytic reactions*, Springer, New York, 2005, pp. 106–137.

70 I. Chorkendorff and J. M. Niemantsverdriet, *Concept of modern Catalysis and Kinetics*, Wiley-VCH Verlag GmbH & Co. KGaA, 2005, pp. 23–78.